COMMUNICATION

Covalent assembly of a two-dimensional molecular "sponge" on a Cu(111) surface: confined electronic surface states in open and closed pores†

Aneliia Shchyrba,[a] Susanne C. Martens,[ab] Christian Wäckerlin,‡[c] Manfred Matena,[a] Toni Ivas,[a] Hubert Wadepohl,[b] Meike Stöhr,[d] Thomas A. Jung*[c] and Lutz H. Gade*[b]

We present a new class of on-surface covalent reactions, formed between diborylene-3,4,9,10-tetraaminoperylene and trimesic acid on Cu(111), which gives rise to a porous 2D-'sponge'. This aperiodic network allowed the investigation of the dependence of electron confinement effects upon pore size, shape and even in partial confinement.

Covalent coupling reactions between molecular units adsorbed at surfaces have recently received increasing attention, in particular in the context of two-dimensional (2D) networks.[1] The most established approaches include Ullman coupling,[1a,b,d–f,2] Schiff base reaction,[3] Glaser coupling,[4] click-reaction[5] or polyester condensation.[6] The synthesis of covalently linked oligo- or polymeric structures is based on the coupling between planar polyfunctional building blocks which require a connectivity greater than two to form 2D assemblies. There are only a few examples of boron-based covalent chemistry to form aperiodic 2D networks.[7]

We previously reported the synthesis of *N,N′;N″,N‴*-diborylene-3,4,9,10-tetraaminoperylene derivatives (**DIBOTAPs**), which contain two borylene groups (BR) (Fig. 1).[8] The parent compound (R = H) **1** was found to react readily with alcohols and carboxylic aids (R–OH), eliminating H_2 and forming B–O–R bonds. This clean coupling along with the elimination of a gaseous co-product (H_2) was thought to provide the basis for an on-surface synthesis of polymeric structures. In combination with a trifunctional carboxylic acid, such
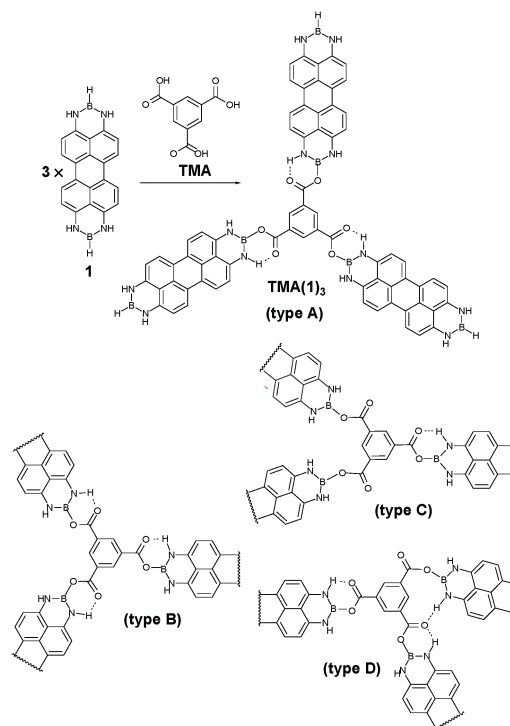

Fig. 1 *N,N′,N″,N‴*-Diborylene-3,4,9,10-tetraaminoperylene (**1**) and benzene-1,3,5-tricarboxylic acid (**TMA**) on Cu(111) form **TMA(1)₃** by covalent reaction after thermal activation at ∼120 °C. The length of **1** is HB–BH 13.724 Å; B–B 11.433 Å and the width is H3–H9 6.564 Å; H2A–H8 6.570 Å (X-ray diffraction study in the ESI†). The flexibility of the covalent link formed by **TMA** deprotonation allows for a wide range of bonding geometries categorized as **types A–D**.

as trimesic acid (**TMA**), the linear **DIBOTAP** could couple to give a porous surface network. The relative angular flexibility of the C(O)–O–B junctions between the building blocks allows for the pore formation of variable size (and shape), resulting in a 'sponge'-like covalent polymer.

Two-dimensional networks provide confinements for the scattering of electrons localized in the Shockley type surface state on noble metal (111) surfaces. Whereas the interaction

[a] Department of Physics, University of Basel, Klingelbergstrasse 82, 4056 Basel, Switzerland. E-mail: aneliia.shchyrba@unibas.ch

[b] Anorganisch-Chemisches Institut, Universität Heidelberg, Im Neuenheimer Feld 270, 69120 Heidelberg, Germany. E-mail: lutz.gade@uni-heidelberg.de

[c] Laboratory for Micro- and Nanotechnology, Paul Scherrer Institute, 5232 Villigen PSI, Switzerland. E-mail: thomas.jung@psi.ch

[d] Zernike Institute for Advanced Materials, University of Groningen, Nijenborgh 4, 9747 AG Groningen, The Netherlands

with small scatterers (*e.g.* metal atoms) is well established,[9] the scattering and confinement mechanisms for 2D molecular architectures[10] are less understood. Therefore it is desirable to create a sample with coexisting pores of different size and shape, which are formed by the same polymer backbone. The investigation of the confined surface states in different open and closed pores by scanning tunnelling spectroscopy (STS) allows to draw conclusions regarding the size and shape dependence of the confinement effect.

Deposition of **1** and then **TMA** on Cu(111) at room temperature (RT) and subsequent annealing at ~120 °C resulted in the formation of porous networks (Fig. 2a, experimental details in ESI†). The pores of the network exhibited different shapes, as expected in view of the flexibility of the intermolecular joints discussed above. At least six different pore geometries could be identified as sketched in Fig. 2d (*cf.* Fig. S4, ESI†). Notably, the same type of network can also be formed under analogous preparation conditions on the less reactive Ag(111) substrate (*cf.* Fig. S5, ESI†).

In order to determine the chemical integrity of the on-surface polymer we probed the chemical environment of C, N, O and B atoms of both **TMA**, **1** as well as of the {**TMA(1)₃**} polymer by XPS (Fig. 2b and c). The C1s and N1s spectra are displayed in Fig. S2 (ESI†) and all XPS peak positions are summarized in Table S1 (ESI†). The unreacted compound **1** gives rise to N1s and B1s peaks at binding energy (BE) of 399.4 eV and 190.2 eV, respectively. For the native **TMA** molecule on Cu(111) two O1s peaks are observed at 531.6 eV and 533.5 eV. The signal at lower (higher) BE is assigned to oxygen in the carbonyl (hydroxyl) group. The observed ratio between the two oxygen species is different from 1:1 due to partial deprotonation of the COOH-groups after **TMA** adsorbs on Cu(111).[11] The on-surface {**TMA(1)₃**} polymer is identified by a

shift (+1.35 eV) of the B1s peak towards higher binding energy (Fig. 2b). This upshift is attributed to the significant difference in electronegativity between boron and oxygen leading to a partial positive charge on boron after formation of the O–B bond. Moreover, the O1s spectra clearly show a modified balance of the two oxygen species corresponding to C–O–B (533.3 eV) and C=O (532 eV) after polymerisation (Fig. 2c). The position of the N1s peak on the other hand remains unmodified (399.4 eV) (*cf.* Fig. S2, ESI†). Thus, the XPS analysis confirms the formation of an on-surface polymer based on covalent oxygen boron (O–B) bonds.

The 2D network acts as a system of different quantum wells interacting with the surface state electrons. Scattering at the ad-polymer can be clearly observed by the standing wave patterns in the STM data shown in Fig. 2a. For a further in-depth analysis of the quantum confinement effects we used scanning tunnelling spectroscopy (STS) at 5 K to probe the local (electronic) density of states (LDOS). The dI/dV spectrum, taken in the center of a certain pore, reveals a confined electronic surface state characterized by a peak energy dependent on the pore dimension (Fig. 3). Note that occupied and unoccupied states are probed at negative and positive sample bias voltage, respectively. The Cu(111) surface state is detected at −450 mV[12] with respect to the Fermi level (E_F) (red curve in Fig. 3a). The following peak values were measured by STS for the different sized and shaped pores: square −90 mV, parallelogram −180 mV, pentagon −265 mV, hexagon −336 mV, heptagon −360 mV and octagon −382 mV (Fig. 3a).

The pore confines the surface state electrons which are free in 2D on the extended Cu(111) substrate. In the following the energies E of the different confined states are referred to the onset of the native surface state E_0. These energies $E' = E - E_0$ are known to scale linearly with the inverse area (1/A) as $E' = C/A$ with $C = \alpha_1 \hbar^2 \pi/(2m^\star)$[13] Here $m^\star = 0.38\ m_e$[12] is the effective electron mass (note, exact value of $m^\star$ slightly deviates in literature, 0.41 m_e[14]) and α_1 is a shape-dependent parameter for the first confined state. Thus, we plot E' *vs.* 1/A (Fig. 3b). Since the shape-dependence for the first confined state is rather small (~9% between square and circle), we employ here for a first approximation the value of a circular pore ($\alpha_1 = 5.783$).[13] This yields a calculated slope $C_{calc} = 1.82$ eV nm² (Fig. 3b, dashed blue line) which does not
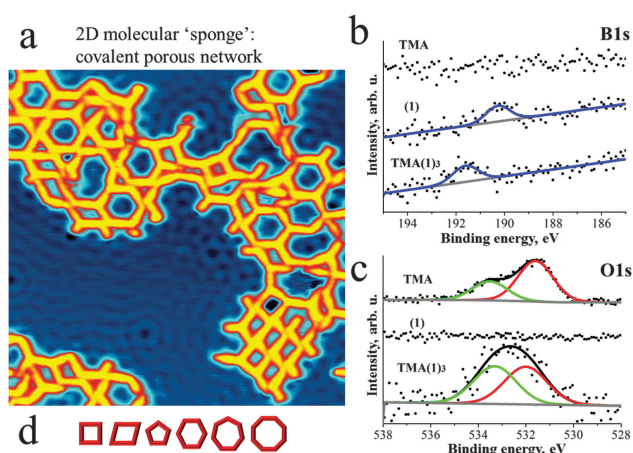
Fig. 2 Deposition of **TMA** and **1** on Cu(111) at RT and subsequent annealing to 120 °C leads to the formation of an aperiodic covalent molecular network {**TMA(1)₃**}. (a) STM micrograph taken at 5 K depicts pores of different size and shape (30 × 30 nm²). Scattering of surface state electrons leads to standing wave patterns on the substrate. (b) The XP spectra of **TMA**, **1** and **TMA(1)₃** reveal a significant shift (+1.35 eV) of the B1s peak towards higher binding energy and (c) the change of the ratio between O1s peaks upon the thermally activated formation of the covalent network. These observations strongly support the formation of a covalent O–B bond in the on-surface polymer, as sketched in Fig. 1. (d) Schematic representation of the various pore sizes and shapes.
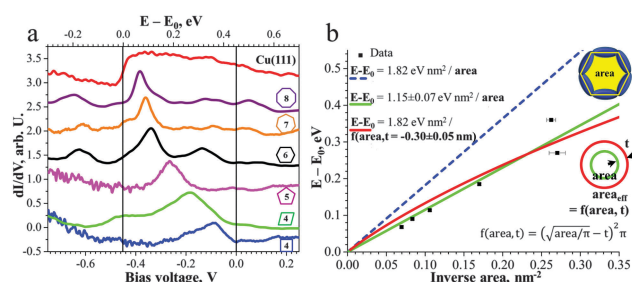
Fig. 3 The porous molecular network on Cu(111) locally confines the surface state and leads to quantum well states with their characteristics depending on the size and shape of the pore. (a) The dI/dV plot of the spectroscopy data reflects the shift of the surface state towards the Fermi level with decreasing pore size. (b) The plot of the energy *versus* the inverse area reflects a linear characteristic for the quantum well state in the confinement. The error bars reflect the average error during defining of the area from the STM image.

agree well with the experimental data or its fitted slope $C_{fit} = 1.15$ eV nm^2 (Fig. 3b, solid green line). Indeed, the effective area occupied by the confined surface state may deviate from the measured (from the center of the molecular backbones) area, as in case of surface states confined by monoatomic steps.[9c] Thus, we fit the data with an effective area which may be smaller or greater by a perimeter t (indicated in Fig. 3b). We find that if the slope C is kept fixed to the value of C_{calc} this yields $t = -0.30$ nm, *i.e.* that the effective area extends by 0.3 nm beyond the molecular backbone. This result indicates that the barrier height is small enough to allow for a considerable penetration of the surface-state even beyond the center of the molecular backbone as observed earlier for a different porous network.[10c]

The "imperfections" of the pore structures in the 2D polymer sponge also allowed us to study the behaviour of the surface state electrons inside a partial confinement, *i.e.* inside "pores" with missing borders. In fact we observed significant electron confinement inside the hexagonal pores even if barriers are missing (Fig. 4). To the best of our knowledge such results have not been reported previously. Comparison of the STS peak-positions recorded in the centre of the closed hexagonal pore as well as in the centre of the pore with 1 and 2 missing barriers reveals the same position (~ -340 mV). By opening the barriers, however, a broadening of the STS peak (Fig. 4b) is evident, which we attribute to interference between partially confined and free 2D electrons. These findings suggest that the size of the pore plays an important role in defining the electronic characteristics of the quantum well state.

We have shown that the flexible covalent linkage formed upon coupling of **DIBOTAP** and **TMA** (liberating H$_2$) allows for the formation of a nanoporous sponge-like 2D-network. The C–O–B bond formation, which gives rise to this surface network, was previously also found to occur in solution.[8] The network forms pores of different architecture, in particular size, shape and symmetry which provides an interesting model system for the investigation of the confinement of Shockley type surface state electrons in a wide range of porous confinements. As expected, decreasing the surface area of the polygon shifts the confined state towards the Fermi level. Interestingly, this work

provides further evidence that the confinement by polymer networks is not perfect. Furthermore, we analysed the confinement effects in open hexagonal pores with a varying number of absent side-walls or barriers. Notably, as shown here for the first time, the confined state energy remains identical to the intact pore. The removal of barriers leads to a broadening of the observed electronic quantum well state. Future work aims at employing modified building blocks to restrict the flexibility of the linker and thus to gain greater control of the porous on-surface architecture.

Notes and references

1 (a) T. Lin, X. S. Shang, J. Adisoejoso, P. N. Liu and N. Lin, *J. Am. Chem. Soc.*, 2013, **135**, 3576–3582; (b) M. El Garah, J. M. MacLeod and F. Rosei, *Surf. Sci.*, 2013, **613**, 6–14; (c) Y.-Q. Zhang, N. Kepčija, M. Kleinschrodt, K. Diller, S. Fischer, A. C. Papageorgiou, F. Allegretti, J. Björk, S. Klyatskaya, F. Klappenberger, M. Ruben and J. V. Barth, *Nat. Commun.*, 2012, **3**, 1286; (d) S. Schlögl, W. M. Heckl and M. Lackinger, *Surf. Sci.*, 2012, **606**, 999–1004; (e) L. Lafferentz, V. Eberhardt, C. Dri, C. Africh, G. Comelli, F. Esch, S. Hecht and L. Grill, *Nat. Chem.*, 2012, **4**, 215–220; (f) M. Bieri, M.-T. Nguyen, O. Gröning, J. Cai, M. Treier, K. Aït-Mansour, P. Ruffieux, C. A. Pignedoli, D. Passerone, M. Kastler, K. Müllen and R. Fasel, *J. Am. Chem. Soc.*, 2010, **132**, 16669–16676; (g) D. F. Perepichka and F. Rosei, *Science*, 2009, **323**, 216–217; (h) M. Matena, T. Riehm, M. Stöhr, T. A. Jung and L. H. Gade, *Angew. Chem., Int. Ed.*, 2008, **47**, 2414–2417; (i) A. Gourdon, *Angew. Chem., Int. Ed.*, 2008, **47**, 6950–6953.

2 L. Grill, M. Dyer, L. Lafferentz, M. Persson, M. V. Peters and S. Hecht, *Nat. Nanotechnol.*, 2007, **2**, 687–691.

3 L. Xu, X. Zhou, Y. Yu, W. Q. Tian, J. Ma and S. Lei, *ACS Nano*, 2013, **7**, 8066–8073.

4 H.-Y. Gao, H. Wagner, D. Zhong, J.-H. Franke, A. Studer and H. Fuchs, *Angew. Chem., Int. Ed.*, 2013, **52**, 4024–4028.

5 (a) P. Fesser, C. Iacovita, C. Wäckerlin, S. Vijayaraghavan, N. Ballav, K. Howes, J.-P. Gisselbrecht, M. Crobu, C. Boudon, M. Stöhr, T. A. Jung and F. Diederich, *Chem. – Eur. J.*, 2011, **17**, 5246–5250; (b) F. Bebensee, C. Bombis, S.-R. Vadapoo, J. R. Cramer, F. Besenbacher, K. V. Gothelf and T. R. Linderoth, *J. Am. Chem. Soc.*, 2013, **135**, 2136–2139; (c) O. Díaz Arado, H. Mönig, H. Wagner, J.-H. Franke, G. Langewisch, P. A. Held, A. Studer and H. Fuchs, *ACS Nano*, 2013, **7**, 8509–8515.

6 A. C. Marele, R. Mas-Ballesté, L. Terracciano, J. Rodríguez-Fernández, I. Berlanga, S. S. Alexandre, R. Otero, J. M. Gallego, F. Zamora and J. M. Gómez-Rodríguez, *Chem. Commun.*, 2012, **48**, 6779–6781.

7 (a) N. A. A. Zwaneveld, R. Pawlak, M. Abel, D. Catalin, D. Gigmes, D. Bertin and L. Porte, *J. Am. Chem. Soc.*, 2008, **130**, 6678–6679; (b) T. Faury, F. Dumur, S. Clair, M. Abel, L. Porte and D. Gigmes, *CrystEngComm*, 2013, **15**, 2067–2075.

8 T. Riehm, G. De Paoli, H. Wadepohl, L. De Cola and L. H. Gade, *Chem. Commun.*, 2008, 5348–5350.

9 (a) M. F. Crommie, C. P. Lutz and D. M. Eigler, *Science*, 1993, **262**, 218–220; (b) K.-F. Braun and K.-H. Rieder, *Phys. Rev. Lett.*, 2002, **88**, 096801; (c) J. Li, W.-D. Schneider, R. Berndt and S. Crampin, *Phys. Rev. Lett.*, 1998, **80**, 3332–3335.

10 (a) P. Han and P. S. Weiss, *Surf. Sci. Rep.*, 2012, **67**, 19–81; (b) L. Gross, F. Moresco, L. Savio, A. Gourdon, C. Joachim and K.-H. Rieder, *Phys. Rev. Lett.*, 2004, **93**, 056103; (c) J. Lobo-Checa, M. Matena, K. Müller, J. H. Dil, F. Meier, L. H. Gade, T. A. Jung and M. Stöhr, *Science*, 2009, **325**, 300–303; (d) F. Klappenberger,
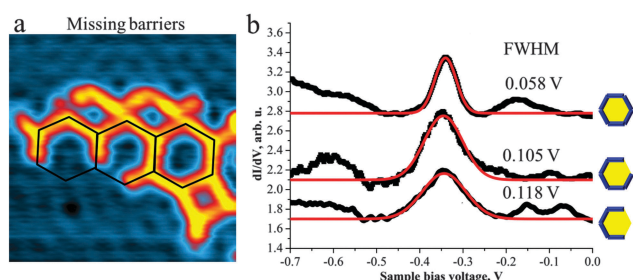

Fig. 4 The dimensions of the **TMA(1)₃** pore determine the energy of the surface state confined inside: (a) hexagonal **TMA(1)₃** pores with missing barriers (STM image: 12×12 nm^2) confine the surface state in considerable similarity to a full hexagon. (b) The dI/dV curves for closed pores and for open pores with 1-, 2-barriers missing reveal the same peak position (~ 0.340 eV). The peak width is increasing with increasing number of absent barriers.

D. Kühne, W. Krenner, I. Silanes, A. Arnau, F. J. García de Abajo, S. Klyatskaya, M. Ruben and J. V. Barth, *Nano Lett.*, 2009, **9**, 3509–3514; (*e*) F. Klappenberger, D. Kühne, W. Krenner, I. Silanes, A. Arnau, F. J. García de Abajo, S. Klyatskaya, M. Ruben and J. V. Barth, *Phys. Rev. Lett.*, 2011, **106**, 026802; (*f*) R. Stiufiuc, L. M. A. Perdigão, B. Grandidier, D. Deresmes, G. Allan, C. Delerue, D. Stiévenard, P. H. Beton, S. C. Erwin, M. Sassi, V. Oison and J.-M. Debierre, *Phys. Rev. B*, 2010, **81**, 045421; (*g*) S. Wang, W. Wang, L. Z. Tan, X. G. Li, Z. Shi, G. Kuang, P. N. Liu, S. G. Louie and N. Lin, *Phys. Rev. B*, 2013, **88**, 245430.

11 (*a*) S. Stepanow, T. Strunskus, M. Lingenfelder, A. Dmitriev, H. Spillmann, N. Lin, J. V. Barth, C. Wöll and K. Kern, *J. Phys. Chem. B*, 2004, **108**, 19392–19397; (*b*) J. V. Barth, J. Weckesser, N. Lin, A. Dmitriev and K. Kern, *Appl. Phys. A: Mater. Sci. Process.*, 2003, **76**, 645–652.

12 M. F. Crommie, C. P. Lutz and D. M. Eigler, *Nature*, 1993, **363**, 524–527.

13 E. Lijnen, L. Chibotaru and A. Ceulemans, *Phys. Rev. E*, 2008, **77**, 016702.

14 F. Reinert, G. Nicolay, S. Schmidt, D. Ehm and S. Hüfner, *Phys. Rev. B*, 2001, **63**, 115415.